Nuclear Instruments and Methods in Physics Research A 1082 (2026) 171031

Contents lists available at ScienceDirect

Nuclear Inst. and Methods in Physics Research, A

journal homepage: www.elsevier.com/locate/nima

Manufacturing & welding feasibility study of the high brilliance neutron source tantalum Target

Y. Bessler [a,*], W. Behr [a], S. Rath [a], J. Wolters [a], J. Baggemann [b], Q. Ding [b], P. Zakalek [b], G. Natour [a,c]

[a] Forschungszentrum Juelich GmbH, Institute of Technology and Engineering (ITE), Wilhelm-Johnen-Strasse, Juelich, 52428, Germany
[b] Forschungszentrum Juelich GmbH, Jülich Centre for Neutron Science (JCNS), Wilhelm-Johnen-Strasse, Juelich, 52428, Germany
[c] ISF Faculty of Mechanical Engineering, RWTH Aachen University, 52062, Aachen, Germany

ARTICLE INFO

Keywords:
HiCANS
High power neutron target
High brilliance neutron source HBS

ABSTRACT

The aim of the High Brilliance Neutron Source (HBS) project is to develop a High-Current Accelerator-driven Neutron Source (HiCANS), which is planned to be built at the Forschungszentrum Juelich GmbH. These types of neutron sources are an efficient and cost-effective alternative to existing low- and medium-flux research reactors. Basically, such neutron sources consist of three main parts: the particle accelerator, the Target-Moderator-Reflector unit (TMR) and the neutron scattering instruments. The Target is of particular importance when designing a neutron source. It must withstand enormous heat stress due to the particle-interactions and is exposed to radiation damage. Moreover, it is usually made of materials that are difficult to manufacture, and which require special weld techniques to join the components. The subject of this publication is therefore the manufacturing and welding feasibility study of the HBS Target prototype made of tantalum. It includes a brief description of the chosen microchannel cooling structure and the thermo-mechanical design of the Target. The results of the welding tests and qualification using special joining techniques like explosion welding of bimetal adapters and electron beam welding of tantalum parts are also presented, as well as the quality verification by destructive and non-destructive testing. Finally, a full-scale manufacturing test of the HBS tantalum Target will be presented.

1. Introduction

Neutrons have been obtained using neutron sources for more than seventy years and are used as probes to study matter. Their physical properties make it possible to study the internal structure and dynamics of matter at the atomic level in a way that is not possible with other methods. This allows the study of the arrangement of atoms and molecules, how they move, how they interact with each other and how they combine to form substances. Neutrons can pass through metals and detect light elements that are difficult to detect by e.g. X-rays. They are therefore an important tool in modern scientific research for studying static and dynamic processes at the atomic level.

Neutrons for scientific purposes have so far been released primarily through nuclear fission in research reactors or by spallation reaction in accelerator-driven spallation neutron sources. Spallation neutron sources enable the highest possible neutron brightness, however, they are very costly in construction and operation, which is why they cannot cover the total demand of neutrons. Research reactors, on the other hand, are increasingly being shut down and building new reactors, especially in Europe, is unlikely. Hence, alternatives are needed.

The High Brilliance Neutron Source (HBS) project [1] will attempt to close this gap. In contrast to the high-energy spallation reaction, where proton energies in the range of several GeV are required, the HBS uses the (p, xn) reaction, which takes place at significantly lower primary particle energy of just a few MeV (CANS) up to 100 MeV (HiCANS). The lower operation energy of such facilities saves construction and operation costs especially of the particle accelerator and the shielding and allows a more compact design of the neutron source. Furthermore, less activated material and therefore less remote handling effort, smaller active cells and less disposal costs of nuclear waste are major advantages of such facilities. This opens the potential to build several low-flux CANS and medium-flux HiCANS, which could, in combination with a few spallation sources and reactor-based sources, cover the future total demand of neutrons for scientific use.

* Corresponding author.
E-mail address: y.bessler@fz-juelich.de (Y. Bessler).

https://doi.org/10.1016/j.nima.2025.171031
Received 28 August 2025; Received in revised form 15 September 2025; Accepted 16 September 2025
Available online 18 September 2025

The lower neutron flux of a HiCANS like HBS compared to high-power spallation sources can be at least partially counteracted by optimization of the TMR unit. Especially the neutronic- and mechanical optimization of the Target can significantly improve the performance of the source. Furthermore, even if the heat load of the Target is lower compared to a spallation Target, it is still challenging to find a working cooling concept to handle, in case of HBS, the heat load of 100 kW on the Target surface of 10×10 cm^2. For this reason, a special microchannel cooling structure has been developed, optimized and tested [2,3], which led to a very complex design, that requires special manufacturing and welding techniques. In addition, the neutronic performance of the Target is sensitive to geometry deviations, which is why high demands on manufacturing tolerances are needed [2]. Furthermore, the Target must be replaced approximately once a year due to radiation damage of the tantalum [2]. Hence, the reproducibility of manufacturing is also very important. Therefore, high quality requirements for manufacturing and welding, both in terms of dimensional accuracy and production reproducibility, must be achieved. This feasibility study was performed to verify the above-mentioned requirements.

The following Chapter 2 describes briefly the HBS facility layout, the Target design solution and the cooling concept. Chapter 3 deals with the qualifications of welding processes used for the following Target manufacturing tests. Chapter 4 presents the first full-scale manufacturing test of the final HBS tantalum Target. Finally, the work is summarized in Chapter 5 as well as a brief outlook is given.

2. HBS target design

2.1. HBS facility layout

Fig. 1 shows the layout of HBS. The main components are: The proton beam linear accelerator (p-Linac) with an energy of 70 MeV and a current of 100 mA that is multiplexed to feed the TMR units operated at different frequencies, the three TMR units that offer a pulsed neutron beam at different frequency, pulse duration and neutron spectrum to fulfil the needs of the individual instruments, and 6 to 8 neutron scattering instruments per TMR unit [1].

2.2. TMR unit

Fig. 2 shows a simplified horizontal (left) and vertical (right) section through the center of one of the TMR units. The tantalum Target, in which the (p, xn) reaction is triggered by proton bombardment and thereby fast neutrons are released, is installed inside an L-shaped vacuum tube, made of aluminum, that is directly (windowless) connected to the proton accelerator channel. The proton beam enters the TMR unit from the bottom and hits the horizontal oriented Target in the center of the TMR unit. To provide the required neutron spectrum to the instruments, different types of moderators (H_2O, liquid H_2, solid CH_4), that slow down the fast neutrons released by the Target, are arranged around the Target (shown is only the liquid H_2 moderator in Fig. 2. , right).

The Target and moderators are surrounded by shielding elements, made of several layers of lead and borated polyethylene, with a total

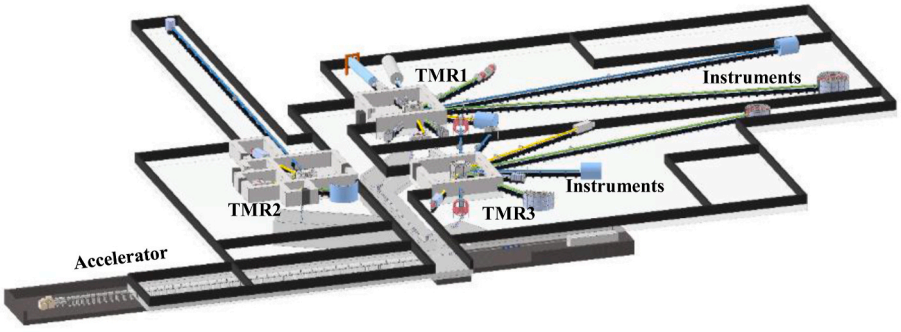

Fig. 1. General layout of the HBS facility [1].

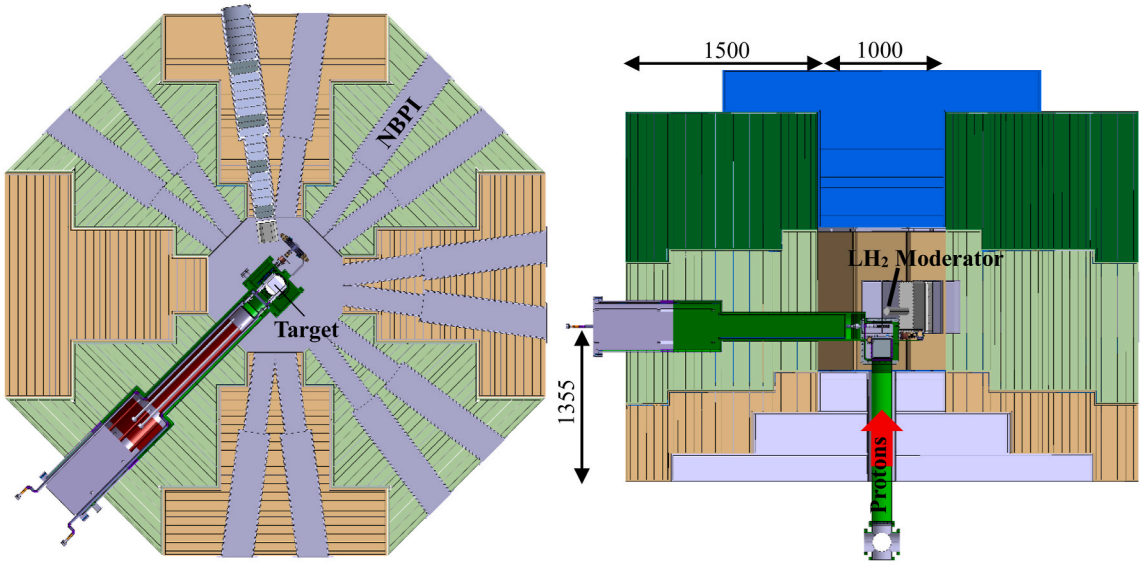

Fig. 2. Simplified horizontal (left) and vertical (right) section through the HBS TMR unit

thickness of 1.5 m. The shielding itself has openings all around for the Neutron Beam Port Inserts (NBPI) and the Target assembly. The NBPIs are adjustable and allow a direct view of the selected moderator and are connected to the neutron guides, which guide the moderated neutrons to the neutron scattering instruments.

2.3. Target assembly

The Target assembly consists of three main parts, shown in Fig. 3. (1) the stepped shielding plug, also made of several layers of lead (grey) and borated polyethylene (red). (2) the Target plug with the tantalum Target on the front side, which is welded to the water-cooling pipes made of aluminum. The pipes are guided inside the stepped aluminum vacuum jacket to the outside of the plug, where they are connected to the main water-cooling loop. (3) the aluminum L-tube, which has CF flanges at both ends, that are bolted to the Target plug on one side and to the accelerator vacuum channel on the other side. Finally, a proton beam diagnostic tool is also foreseen as part of the L-tube assembly, which can be moved between the proton beam and Target while operation to analyze the beam profile for example.

Except for the demountable tantalum Target main body and the reusable Target shielding plug, the entire assembly is made of aluminum, which will be separated from the tantalum body prior to disposal, thus significantly reducing the amount of long-radiating material to be stored. The regular exchange of the Target plug and the separation of tantalum will be done with a special remote handling tool.

2.4. Target material and lifetime

A neutron yield of up to 10^{15} n/s can be achieved for a proton energy of 70 MeV at a current of 1 mA by using heavy elements with atomic numbers of $70<Z<82$ [4]. Along with tungsten, tantalum has, under the given conditions, the best neutron yield of 0.14 neutrons per incoming proton [3]. That leads to a total neutron yield of $8.6{\cdot}10^{14}$ n/s for the HBS [3], which is about two orders of magnitude less than the neutron yield of the world's most powerful source, the European Spallation Source ESS and comparable with the SINQ neutron source at Paul Scherer Institute for example and other medium-flux neutron sources. Another advantage of using tantalum as a Target material is the higher blistering threshold compared to tungsten. All details of the material chosen have been published in the framework of a neutronic-optimization study in Ref. [2]. The lifetime of the Target is driven by the radiation damage of the tantalum. A distinction is made between neutron-induced radiation damage and proton-induced radiation damage, whereby the permitted neutron-induced radiation damage is 0.14 DPA (Displacement Per Atom) [5] and the proton-induced radiation damage is 11 DPA [6] respectively. According to Ref. [2], in case of HBS, the radiation related lifetime is reached after 1.17 years of full power operation, driven by the neutron-induced radiation damage. By comparison, the limit for proton induced radiation damage is reached only after 5.7 years of full power operation. That means that three Targets, one for each TMR unit, per year are needed. Assuming that the operating time of the HBS is 40 years, this would result in the need to manufacture up to 120 Targets.

2.5. Target cooling design

The HBS proton beam accelerator delivers protons with 70 MeV energy, a peak current of 100 mA and a low duty cycle of around 2 %, which results in a time-averaged heat deposition of 100 kW on the Target surface [1]. The irradiated area of the Target is 10×10 cm^2, that leads to a time-averaged heat density of 1 kW/cm^2, which is why an active cooling becomes unavoidable. As a cooling media light water was chosen. Fig. 4 shows the final design of the HBS tantalum Target as a result of several iterations of neutronic and engineering. The result is a compromise between neutronic performance, coolability and manufacturability.

To minimize hydrogen implantation and to reduce the heat load

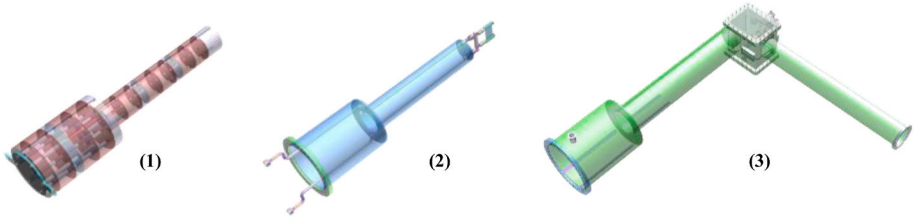

Fig. 3. (1) Target shielding plug, (2) Target plug with tantalum Target, (3) Vacuum L-tube

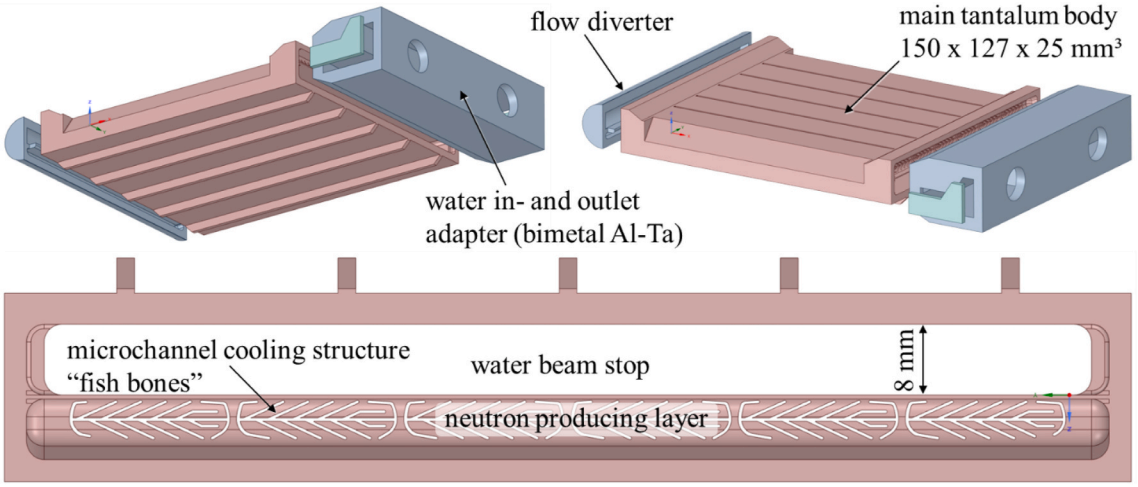

Fig. 4. Design of HBS tantalum Target. Upper figure: isometric view of model front and back side, lower figure: detailed view of microchannel cooling structure and beam stop

deposited inside the tantalum, the proton Bragg peak is positioned in the center of the cooling water backflow, called water beam stop, located on the backside of the neutron producing layer of the Target. Hence the heat generated in the beam stop, which is about 20 % of the total energy that needs to be removed, can directly be transported away by the cooling water without heating up the tantalum. However, the main part of the energy is deposited inside the tantalum and must be removed from there. For this reason, a cooling design based on microchannel cooling structure, forming a few fishbone-shaped sections, was developed [3]. This kind of cooling structure has sufficient heat transfer properties and the best possible ratio of cooling water and tantalum. However, manufacturing is very demanding, and the fine 0.35 mm thick channels are very sensitive to geometric deviations, which is why very tight tolerances must be maintained. The main cooling water flow enters first the bimetal inlet adapter where the flow is split and then enters the microchannels sectors as a parallel flow. At the outlet of the microchannel sectors, the flow is reunited and flows again as a serial flow into the 180° flow diverter on the top of the Target. The flow diverter is also made of tantalum and welded via electron beam welding to the main body. Finally, the flow passes the beam stop on the back side of the Target and exits the assembly. Furthermore, stiffening ribs are implemented on the outside of the beam stop to stabilize the outer wall, that needs to withstand the internal water pressure. To minimize the amount of tantalum, the in- and outlet adapter is made of aluminum where a 2 mm thick layer of tantalum is joint on the front using explosion welding, which in turn is welded to the main body by electron beam welding.

2.6. Thermo-mechanical design

One of the main challenges regarding the Target design is the reliable heat removal capability and sufficient mechanical stability, at the same time considering the requirements regarding the neutronic design and manufacturing issues.

The final Target layout is the result of many iterations of neutronic simulations [2] and coupled thermo-mechanical simulations. In the following, the results of the computational fluid dynamics simulations with ANSYS CFX and thermo-mechanical calculations with ANSYS Mechanical are presented.

Some details of the CFX simulation model are shown in Fig. 5. Here a sufficient fine mesh at the solid-fluid-interfaces is essential for predicting the heat transfer sufficiently accurate, leading to a large model consisting of about 33 million elements in total. Temperature dependent properties for thermal conductivity, viscosity and specific heat capacity according to Ref. [7] were considered for water, while for tantalum a constant specific heat capacity of 140 J/(kg·K) and a mean thermal conductivity of 58 W/(m·K) are used for the simulation [8].

The time-averaged heat deposition for tantalum and water was imported from the particle transport simulation [2]. For tantalum the

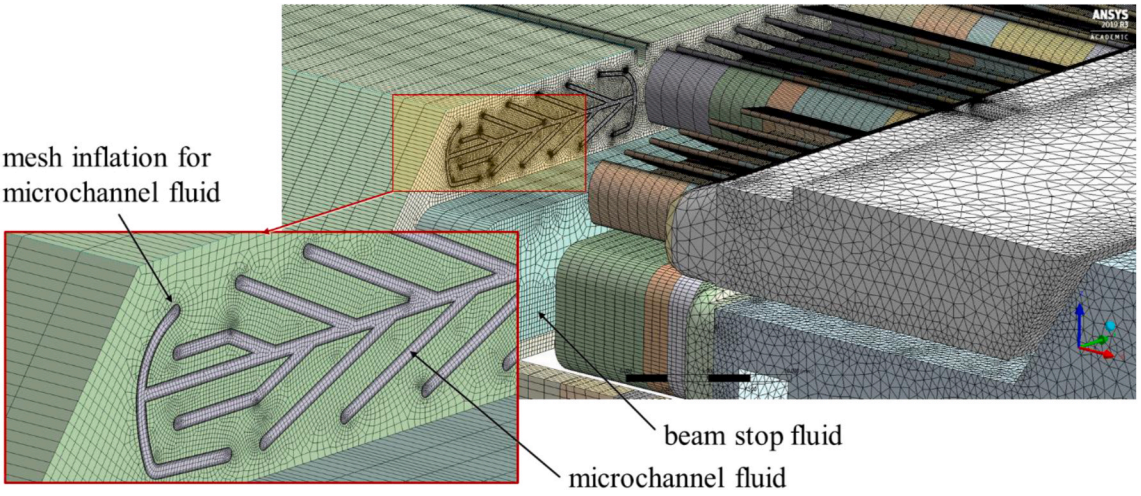

Fig. 5. Simulation mesh of HBS Tantalum Target showing details of the finer resolution at the solid-fluid-interfaces

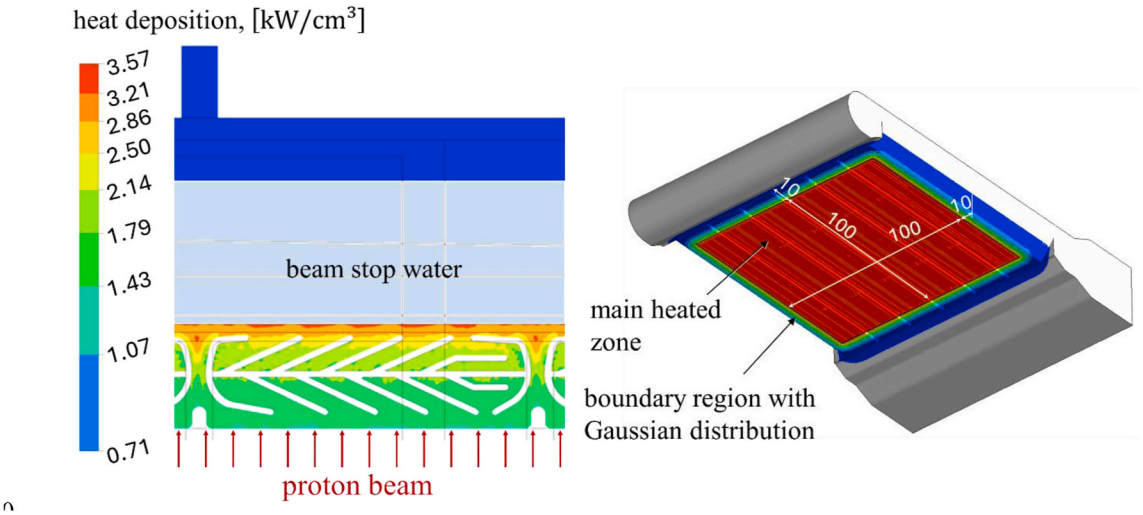

Fig. 6. Time averaged heat deposition in tantalum imported from particle transport simulations (left side) and considered heated zones of the target (right side)

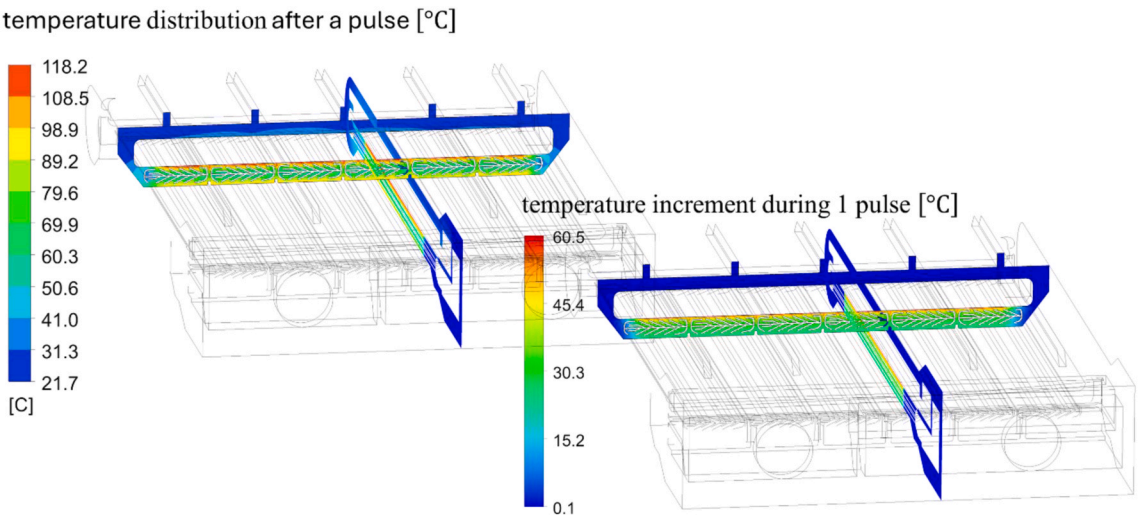

Fig. 7. Temperature results for pulsed operation at 24 Hz and a time-averaged power of 100 kW, left side: temperature distribution after a pulse within relevant cross sections, right side: temperature increment during one pulse

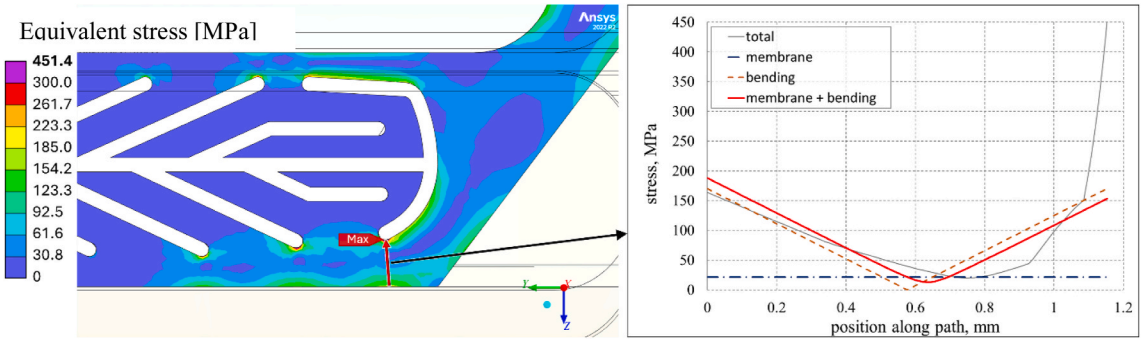

Fig. 8. Primary stresses (left) and bending and membrane stresses (right) in the critical area of the Target

imported data is shown in Fig. 6. Applying this heat deposition to the heated zone and considering a Gaussian drop in a 10 mm large boundary region the total thermal power is about 141 kW and therefore much higher than the design specification of 100 kW. To comply with the specification, the heat input was scaled by a factor of 1/1.41. For cooling water with 20 °C inlet temperature and a mass flow rate of 1.34 kg/s is foreseen, leading to an average velocity in the microchannels of about 8 m/s and a pressure drop of about 3.4 bar. At an inlet temperature of 20 °C, the outlet temperature of the water is approximately 38 °C.

For the transient simulations considering the pulsed operation of the HBS with 24 Hz the time-averaged heat deposition is scaled by the factor 50, which is given by the reciprocal of the pulse duration divided by the duration of one cycle. The transient simulation comprises 13 pulses, whereby the maximum operating temperature was already reached after 7 pulses. The temperature distribution after a pulse is shown in Fig. 7, left side. One reason for the high temperatures occurring for the pulsed operation is the large temperature increment during the pulse (cf. Fig. 7, right side), caused by the rather low pulse frequency and the resulting high energy deposition during one pulse. Nevertheless, the maximum interface temperature within the microchannels will stay below the boiling temperature of water so that the essential cooling within the neutron producing layer of the Target is ensured. At the interface to the water in the beam stop the temperature will exceed the boiling temperature of the water and here nucleate boiling will occur. However, the determined interface temperature is conservative, since the increased heat transfer coefficient for nucleate boiling is not considered in the single-phase calculations. However, to benefit from the increased heat transfer coefficient when boiling occurs, this interface must be orientated upwards to allow the gas bubbles to detach and to avoid accumulation of gas bubbles at the interface, leading to potential film-boiling with worsened heat transfer performance.

With respect to the thermo-mechanical design, two main aspects are relevant. First of all, the water pressure within the beam stop will lead to high primary bending stresses in the Target and especially in the microchannel structure close to the outer sides of the Target. Here local plastic deformations are acceptable as long as the nominal stresses (membrane plus bending stress) of the relevant cross section is below the allowable stress. Secondly, cyclic secondary stresses due to the temperature increments caused by the pulsed operation must not exceed the fatigue strength of the material.

Primary stresses due to the coolant pressure are shown in Fig. 8, left side, for the cross section with the maximum equivalent stress. Although the maximum local stress is 451 MPa and significantly higher than the yield stress of tantalum of about 185 MPa [9], the nominal membrane plus bending stress for the relevant cross section is however only in the range of the yield stress and therefore acceptable.

Moreover, a collapse simulation with ideal-plastic material behavior has shown a safety factor of almost 9 against plastic collapse and of 2.8 against reaching the elongation at break due to the water pressure.

3. Welding qualification

After the thermo-mechanical design has been carried out, joining technologies for the aimed materials must be proved. In principle, solid-state welding and beam welding can be used for the needed tantalum-aluminum bimetal joint and for joining the tantalum main parts.

3.1. Explosion welding

Explosive welding or explosive cladding is a solid-state welding process in which two or more metallic materials can be welded together with the aid of explosives. Explosives were already being used to form and emboss sheet metal around 1890. The fact that explosives are suitable as an energy carrier for welding metallic materials together was observed by chance in 1957 during a failed forming test. In this experiment, an aluminum base was foreseen to be blasted into a steel die, but the base was welded to the die. This can be seen as the beginning of industrial blast welding; the first patents for this process were registered in the years 1959–1962 and from 1963 blast cladded sheet metal was produced on a commercial scale in the USA and from 1968 in Germany. Explosive welding can be used to produce material composites of 0.2 m^2–20 m^2 in a single shot. As is usual with solid-state welding processes, many material combinations that are generally metallurgically incompatible can be joined with this process. In order to create a material bond during explosive cladding, the surfaces of the materials must be brought together at an atomic distance so that atomic forces of attraction can become effective. The oxide layers present on almost every surface initially poses a problem. In conventional cold pressure welding and roll cladding, these are broken up by increasing the surface area. The existing contact pressure ensures plastic flow in the joining zone so that the minimum distance required for a metallic bond is achieved. Explosive welding is characterized by the fact that this takes place under much higher pressure and at significantly higher speeds. Existing oxide layers are removed from the joining zone during the cladding process [10]. Fig. 9 shows the production process for explosion welding.

In the first step (1), the materials are inspected for sufficient evenness. In the next step (2), the surfaces to be joined are cleaned of impurities by grinding and uniform surface qualities are produced. With the help of spacers, the sheets are positioned in relation to each other, and the explosive is applied to the top of the support sheet (3). The spacing, quantity and type of explosive depend on the materials used and are characteristic of the respective material combination. The explosive is activated with the aid of a detonator and a detonation front spreads out. The cladder is accelerated towards the backer and strikes it at an angle (4). The basic prerequisite for a welded joint is that the two surfaces meet at a speed of more than 100 m/s and at an angle of 2°–25°. Under these boundary conditions, a desired plastic flow of the two materials occurs, and a metallic bond is formed. Due to the high process forces, the entire sheet metal package is deformed and must be straightened after the joining process (5). With the subsequent nondestructive tests (NDT) (6), the material bond is checked for bonding. The mechanical and technological properties of the material composite are also checked using destructive testing [11].

3.2. Electron beam welding

Electron beam welding (EBW) in a vacuum chamber is the best joining process for welding heat-resistant metals. The electron beam can be adapted to the geometry and material requirements of the joining zone with the highest precision and a wide variety of process parameters, such as deflection frequency and geometry, focus position, and pulse modulation. The electrons are accelerated up to 2/3 of the speed of light at an acceleration voltage of 120 kV–150 kV and thus melt any electrically conductive material [12].

Especially with high-melting refractory metals, the use of an electron beam is very advantageous. In addition, welding in a vacuum environment prevents contamination of the joining zone by residual gases. For this reason, the pressure in the welding chamber when welding refractory metals should always be $\leq 10^{-4}$ mbar and oil-free vacuum pumps, such as turbomolecular pumps and screw pumps, should be used [13].

Table 1
Analysis of alloy components of tantalum and aluminum (AlMg3).

Sheet for explosive cladding	Ta-426; cold rolled, annealed	Plates for Target and tensile test	Ta-450a; cold rolled, annealed	Plate for explosive cladding	AlMg3 (EN AW-5754)
Ta	99.95 %	**Ta**	99.95 %	Al	
C	20 ppm	**C**	40 ppm	Si	0.18–0.40 %
N	20 ppm	**N**	20 ppm	Fe	0.32–0.40 %
H	10 ppm	**H**	10 ppm	Cu	0.04–0.10 %
O	100 ppm	**O**	80 ppm	Mn	0.47–0.50 %
Ti	10 ppm	**Ti**	5 ppm	Mg	3.30–3.60 %
Nb	90 ppm	**Nb**	80 ppm	Cr	0.07–0.30 %
Fe	30 ppm	**Fe**	1 ppm	Ni	0.010 %
Si	20 ppm	**Si**	1 ppm	Zn	0.07–0.20 %
W	30 ppm	**W**	50 ppm	Ti	0.02–0.15 %
Ni	10 ppm	**Ni**	1 ppm		
Mo	10 ppm	**Mo**	30 ppm		

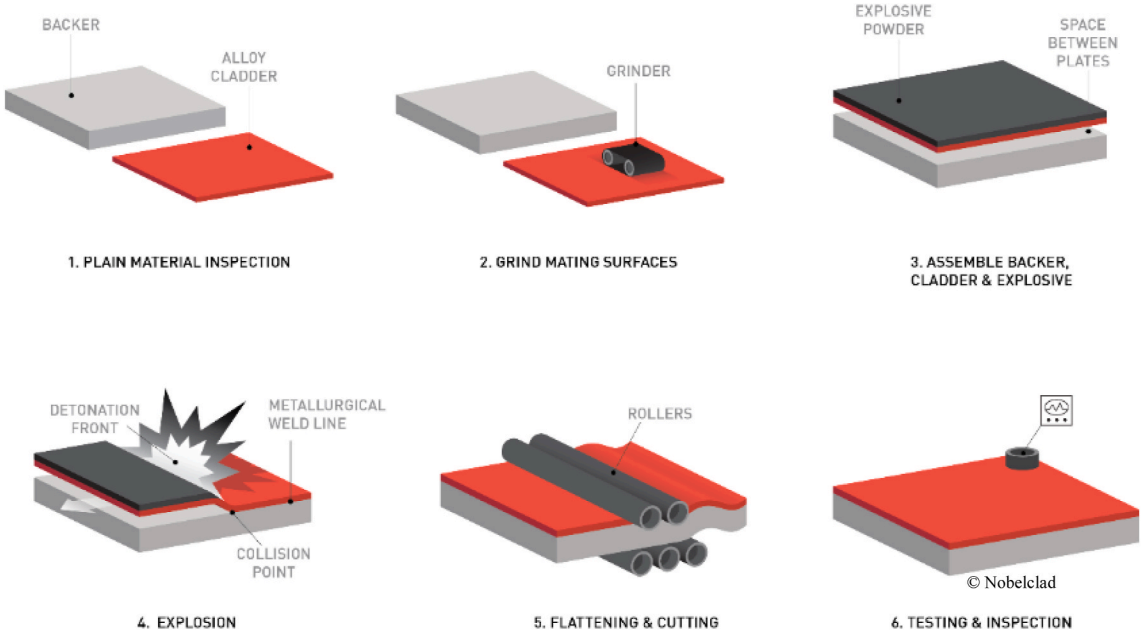

Fig. 9. Production process for Explosion welding [11].

3.3. Analysis of alloy components

Table 1 provides an overview of the impurities in the tantalum and lists the alloy composition of the aluminum alloy used.

3.4. Material properties of tantalum

Even though it has not yet been decided which directive will be used for the mechanical design of the Target, it can be assumed that it will be either the RCC-MRx code [14] or the pressure equipment directive (PED) [15]. However, in both guidelines no material data for tantalum

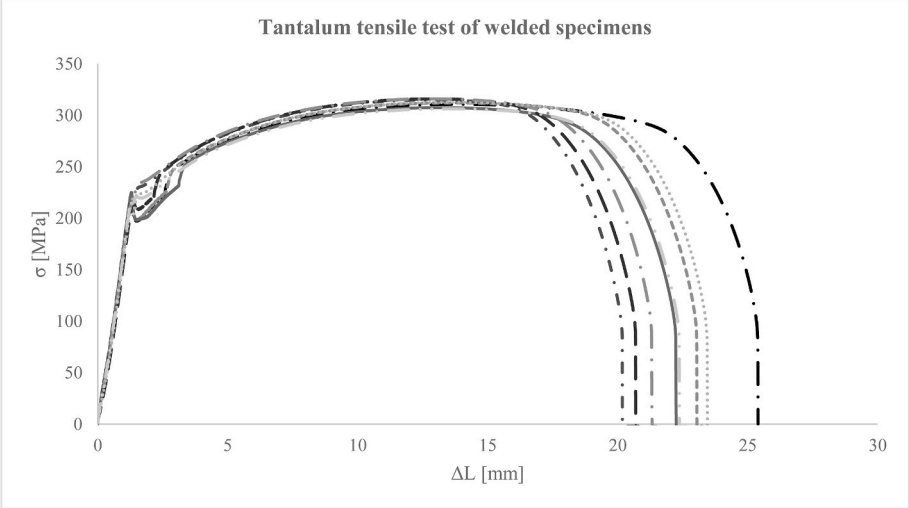

Fig. 10. Tantalum welding tensile test. The different lines show the respective individual measurements

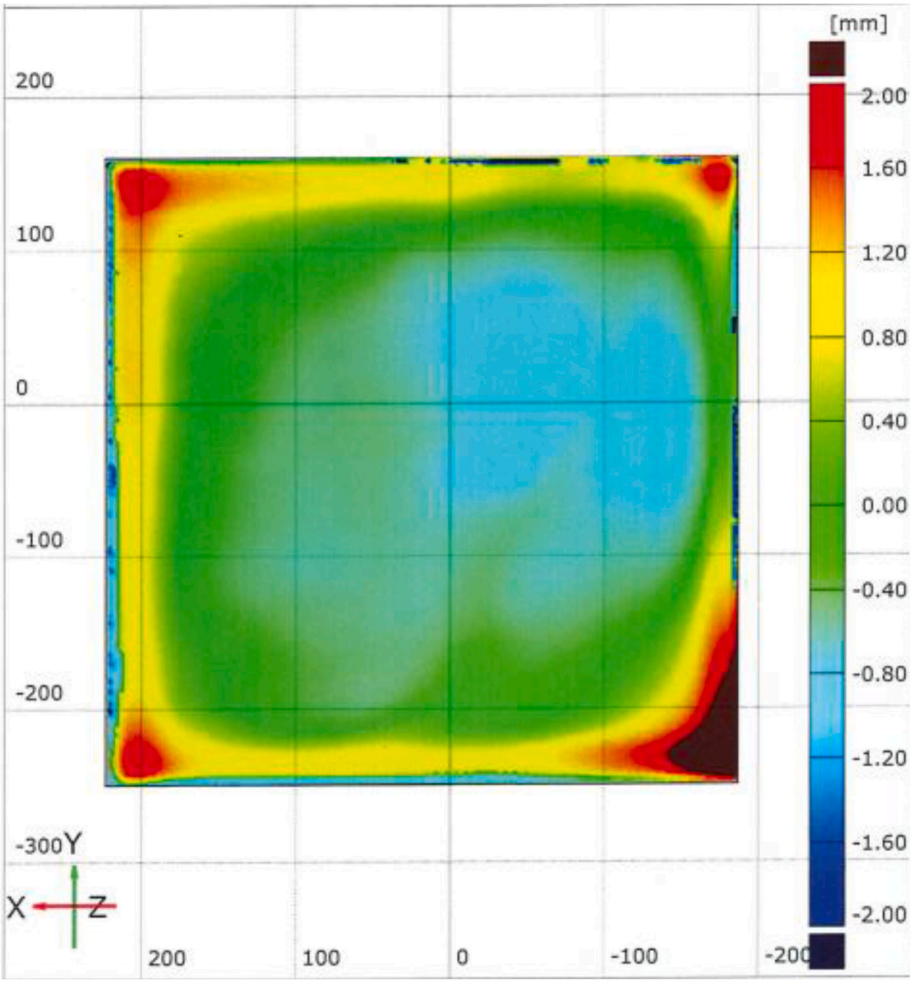

Fig. 11. Dimensional control (flatness) of the explosive-clad plate

can be found, in contrast to AlMg3. In addition, the strength values of tantalum given in data sheets and material libraries vary considerably, which is why experimental determination of the strength values based on the material charge used for the final product becomes necessary. Furthermore, data of welded tantalum is also missing. Therefore, tensile tests of unwelded and welded tantalum were performed.

For this reason, a 5 mm thick tantalum plate was joined using electron beam welding. Tensile specimens were then machined out from the welded plate according to *DIN 50125* tensile specimen form E. In order to compare the results of the tensile test, unwelded samples of the same geometry were also manufactured. Fig. 10 summarize the results of the tensile test.

The average yield strength of welded specimens is $R_p(Ta) = 213.5$ MPa ±1.9 MPa and thus is about 15 % higher than the literature value used for the thermo-mechanical simulation. The average tensile strength of welded specimens is $R_m(Ta) = 312.1$ MPa ±3.4 MPa. The total elongation was measured indirectly via crosshead travel of the tensile machine and is $\varepsilon_0 = 28.2\ \% \pm 1.8\ \%$. The difference to unwelded samples were negligible.

3.5. Dimensional control of the explosive welded plate

For the welding qualification and for the first full scale prototype of the HBS tantalum Target an aluminum (AlMg3) plate with the dimension of 400 x 400 × 40 mm^3 was joined with a tantalum sheet of 400 x 400 × 2 mm^3 by explosive cladding. To ensure that the thickness and the

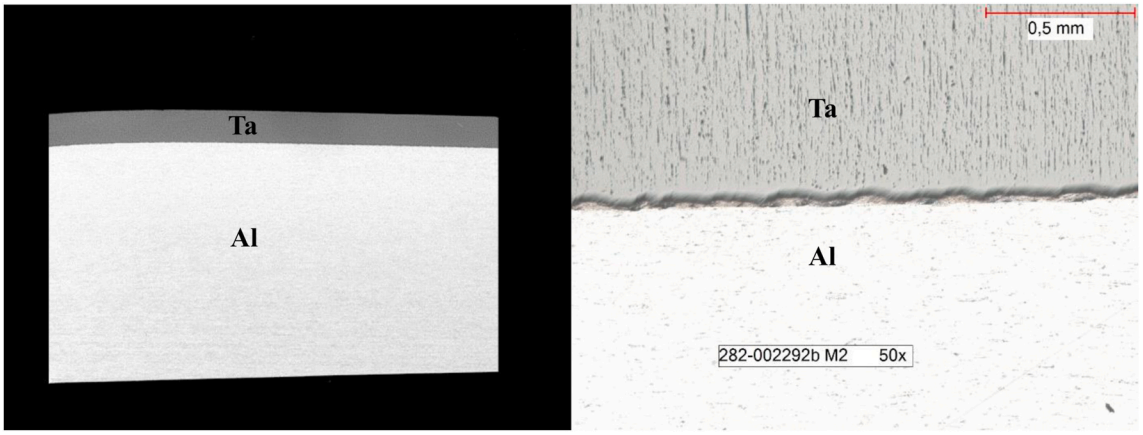

Fig. 12. Macrostructure (left) & Microstructure (right) of bimetal joint

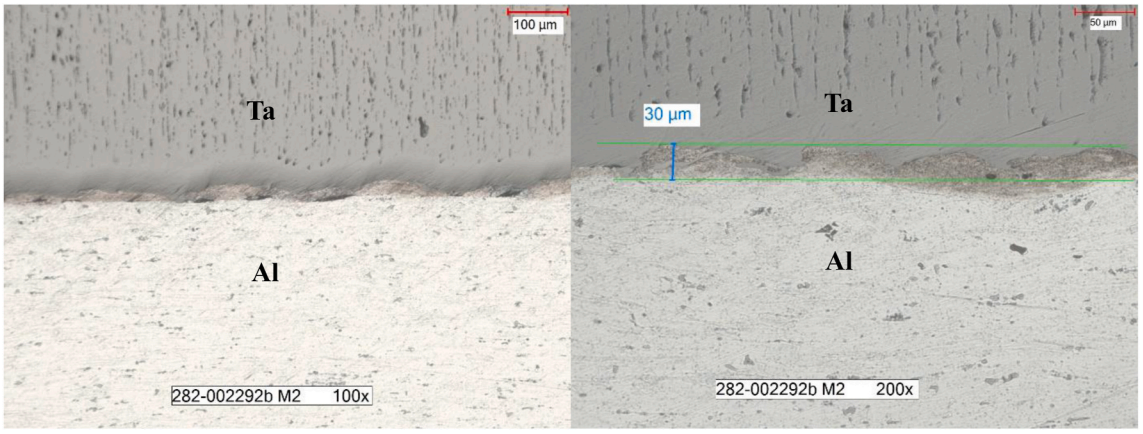

Fig. 13. Microstructure of bimetal joint

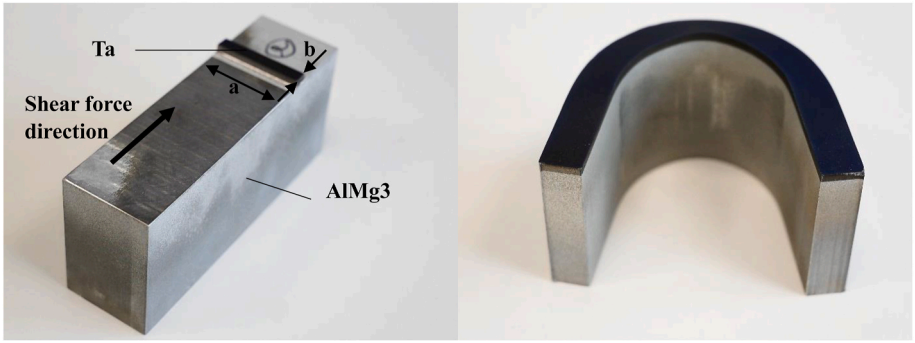

Fig. 14. Shear (left) & bending (right) test samples of the explosive-clad plate

Table 2
Results of shear & bending test of the explosive-clad plate.

	Shear test			Side bend test	
Sample	Fracture surface a·b [mm^2]	Tangential force [N]	Shear strength [MPa]	Crack	No crack
1	24.88·4.51	23900	213		X
2	24.94·4.51	23600	219		X
3	24.99·4.50	22600	201		X
4	23.00·4.50	21000	203		X

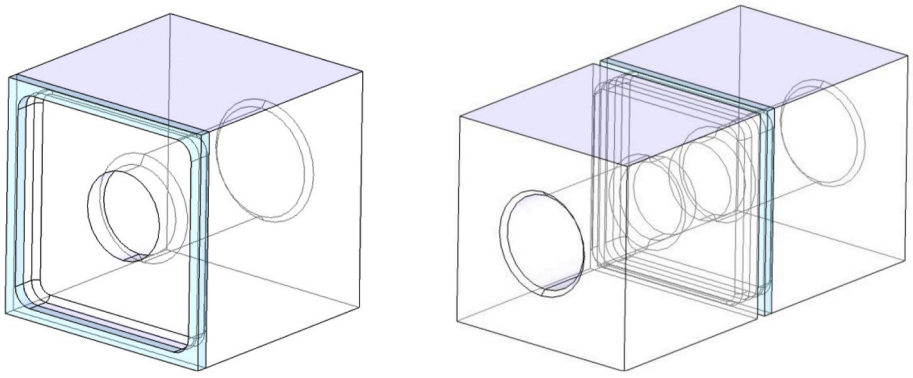

Fig. 15. Sample geometry, tantalum 40 x 40 × 2 mm^3 and AlMg3 40 x 40 × 40 mm^3

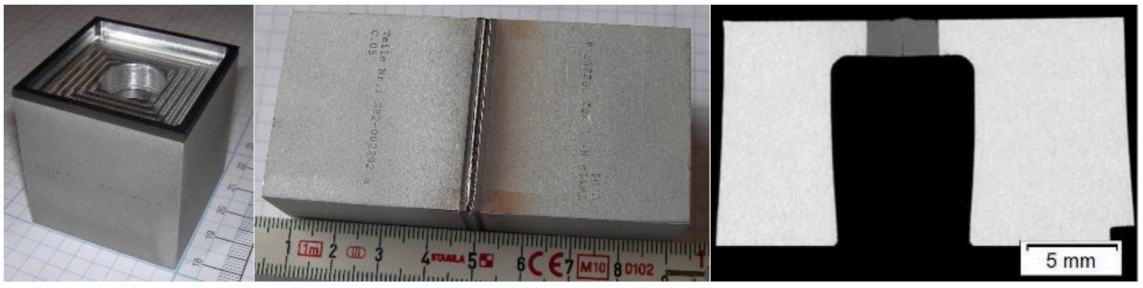

Fig. 16. Al/Ta sample before (left), after welding operation (middle) and cross-sectional view of the Al/Ta sample (right)

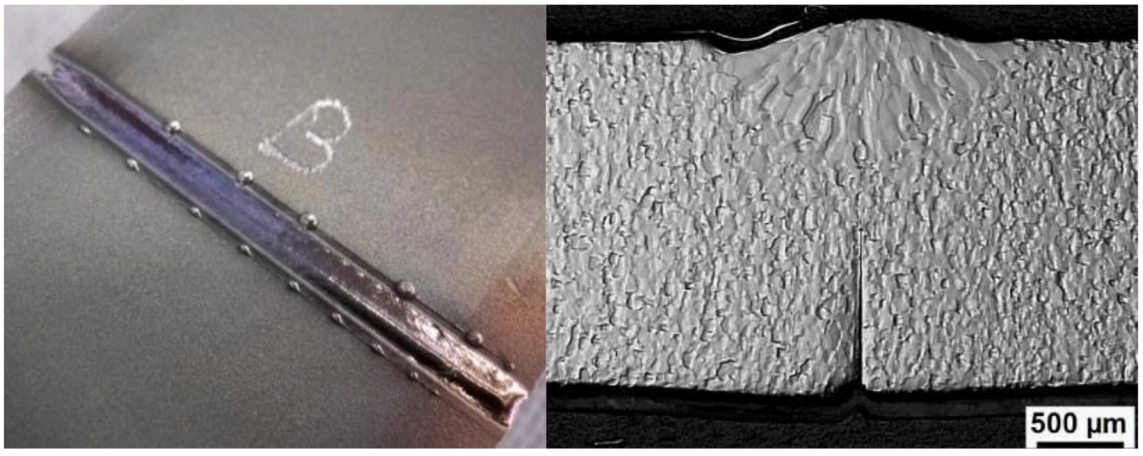

Fig. 17. Cross-sectional examination Al/Ta; electron beam-power 4.9 kW

straightness of the tantalum layer meet the requirements, the plate was first geometrically measured before the samples for welding qualification and the bimetal adapter of the full-scale manufacturing test of the Target were manufactured.

Since EBW requires a high tolerance with regard to straightness and dimensional accuracy, the samples are machined on the front side after cutting. In order to ensure the thickness of the tantalum layer, it is therefore necessary to take samples from areas that show only small deformations. As can be seen in Fig. 11 the deformations, especially in the corner areas, are too large, which is why samples are taken exclusively from the core area (green and light blue areas).

3.6. Macro & micro structural analysis of the explosive welded plate

The macro- and microstructure analysis of welded joints is an essential component of quality assurance. Macroanalysis is used to assess the external shape, geometry, and surface condition of the weld. Microanalysis examines the weld structure at the microscopic level to obtain information about the grain structure, phase composition, and possible structural defects. Both analyses together provide information about the quality of the joint and potential defects.

Fig. 12, shows on the left side the macrostructure of the bimetal plate and on the right side the microstructure with 50x magnification. Clearly visible is here the diffusion zone of the explosive welded Ta/Al bimetal

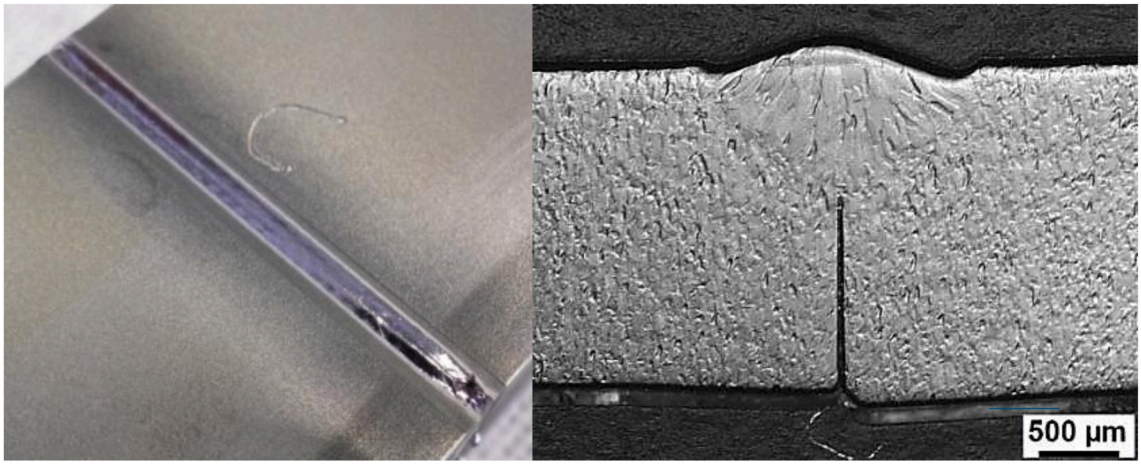

Fig. 18. Cross-sectional examination Al/Ta; electron beam-power 3.2 kW

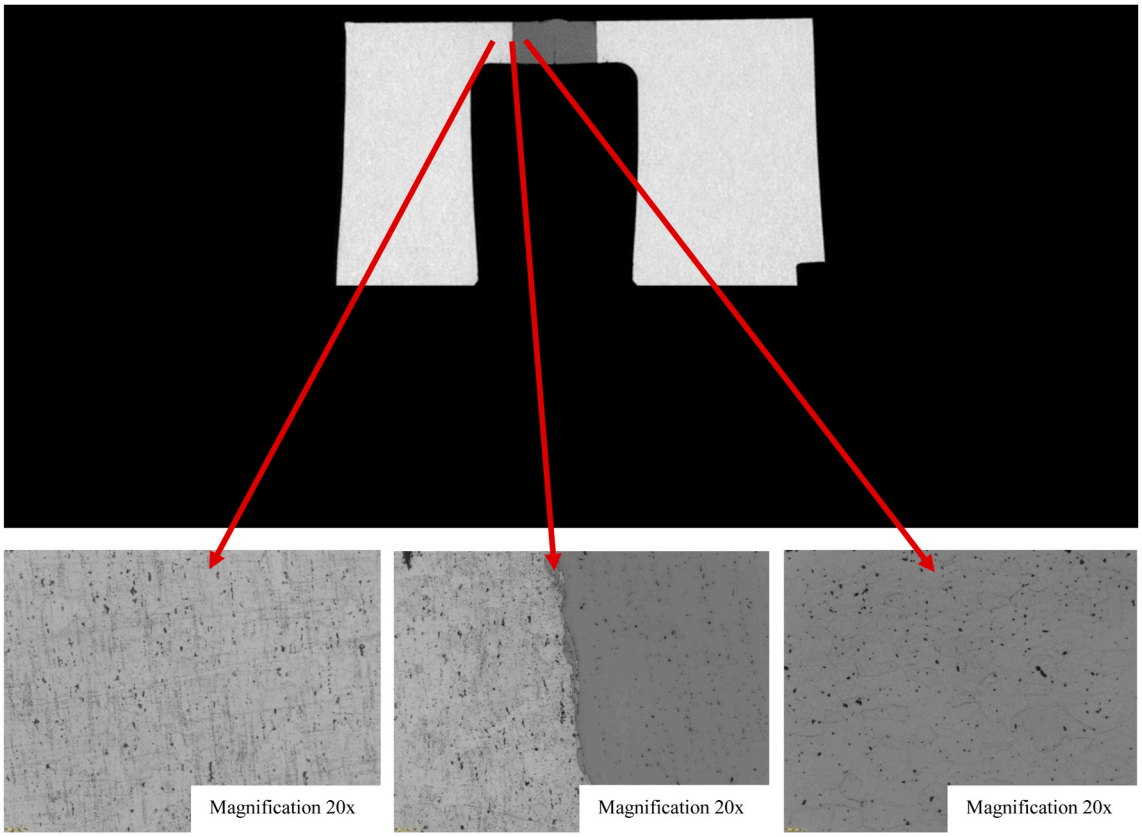

Fig. 19. Cross-section examination of Al/Ta bimetal-layer after electron beam welding; top: macrosection 1:1; left: Al-base metal; middle: heat affected bimetal layer; right: Ta-base metal

plate, with the typical wave structure.

Fig. 13 shows the microstructure of the bimetal joint with 100x magnification on the left and with 200x magnification on the right.

The image on the right shows a detail of the approximately 30 µm thick diffusion zone with higher resolution. No significant binding defects or foreign inclusions can be seen in these images.

In general, the macro- and microstructure examination according to *DIN EN ISO 17639:2022* were without any objection and the explosive welded Ta/Al bimetal plate is therefore suitable for the first HBS Target prototype.

3.7. Shear & bending test of the explosive welded plate

Shear and bending tests are destructive testing methods performed on welded joints or other joints to evaluate their mechanical properties, in particular their resistance to bending and shear forces. Shear tests at joints are important for assessing the load-bearing capacity of the joint under loads that could lead to shearing of the joined parts. The results of the bending test provide material parameters such as the maximum bending stress, occurring deformations, and ultimate strength. The samples used are shown in Fig. 14. For the shear test samples, the tantalum was milled off the bimetallic plate except for a strip of size a x b.

Table 2 summarizes the results of the shear- and bending tests.

The shear strength indicates the maximum shear stress with which a body can be loaded before shearing, i.e. the maximum tangential force relative to the entire fracture surface. In this case, the shear strength is $\tau S = 209$ MPa ± 7.3 MPa and is in the range of the tensile strength of the weaker material (R_m(AlMg3) = 190–240 MPa) and therefore acceptable. In the bending test, the samples were deformed by 180° along the

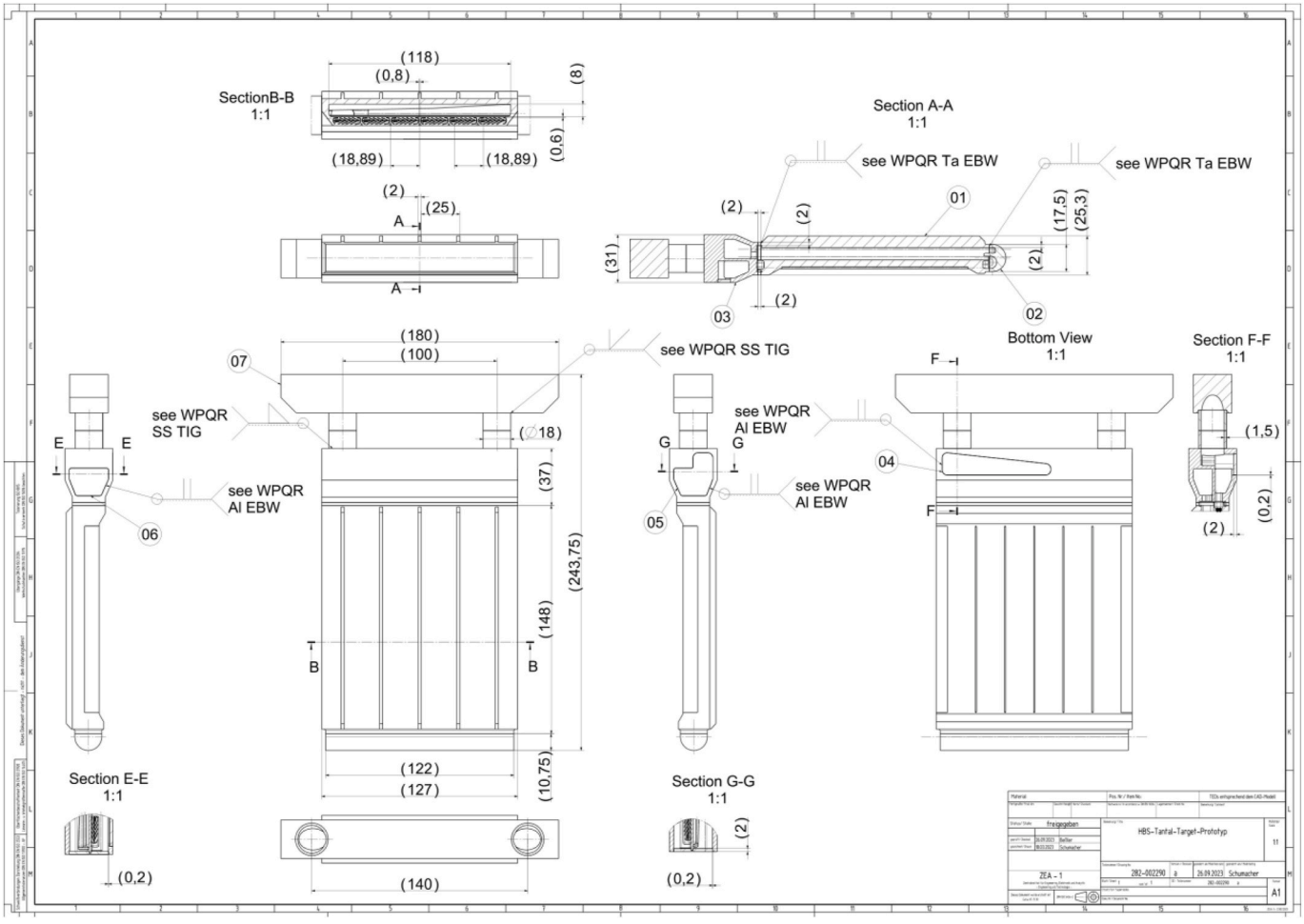

Fig. 20. Welding drawing of HBS tantalum Target prototype

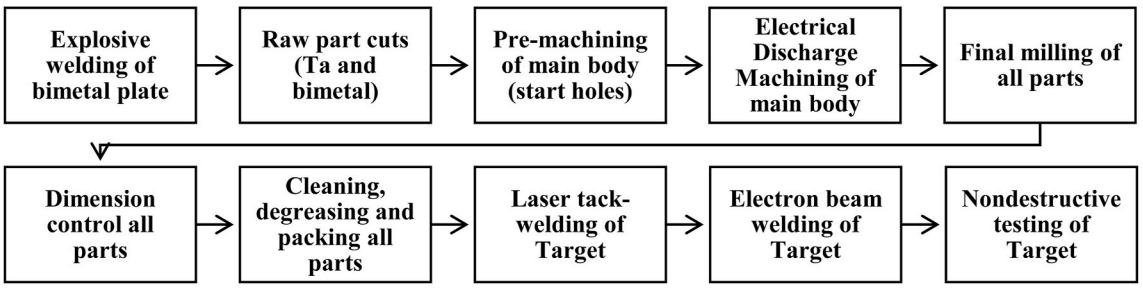

Fig. 21. Manufacturing sequence of HBS tantalum Target prototype

joining zone, whereby the tantalum layer did not detach from the aluminum plate, and no cracks occurred. Therefore, these results are also acceptable.

It should be noted, however, that the influence of irradiation that occurs during the operation of the Target was not considered. This could, especially in the case of the bimetallic joint, reduce the lifetime of the entire Target due to embrittlement and other radiation effects. It is therefore recommended to repeat the same tests with irradiated samples in order to prove the suitability of the bimetal for the HBS Target.

3.8. EBW & explosion welding test

For joining qualifications of both welding processes, test samples were manufactured. The welding sample geometry is shown in Fig. 15. First, cube shaped samples of 40 x 40 × 42 mm^3 were cut out from the explosive welded plate. A central 1/4″ threaded hole was then machined for subsequent pressure and leak tests. Finally, a 4 mm deep pocket was milled out on the tantalum side, leaving a radial wall thickness of 2 mm (as in the original component). Two of these samples were then stacked on top of each other to create a chamber of 8 x 36 × 36 mm^3, see Fig. 15 right.

A manufactured sample is shown in Fig. 16, left. Two of these samples were welded with vacuum electron beam welding to get a provable sample, see Fig. 16, middle.

Due to the very close explosive welded aluminum/tantalum joining zone, the EBW process must be adjusted in such a way that no influence on this zone occurs. The melting point of tantalum of approx. 3000 °C is considerably higher than that of the used Al alloy AlMg3 of approx. 610 °C. In addition, the diffusion zone of the explosion weld could be damaged, which is why the temperature in this region should not exceed 610 °C. Therefore, tantalum welding must be carried out with extremely low energy input. On the other hand, the welding depth should be as close as possible to full penetration of the wall in order to meet the structural mechanical requirements. In addition, a very low leakage rate of the joining zone must be achieved because the Target is surrounded by the accelerator vacuum.

However, already at a welding depth of approximately 1.3 mm, aluminum-melting droplets appear at the tantalum/aluminum border line, as can be seen in Fig. 17, left.

Choosing a lower energy input combined with high welding velocity

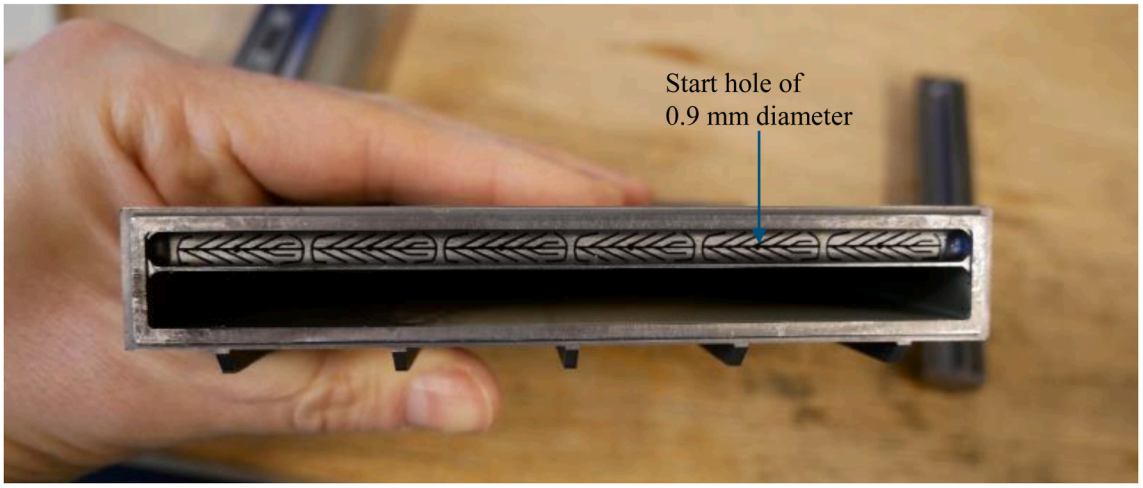

Fig. 22. Wire EDM machined micro channel cooling structure

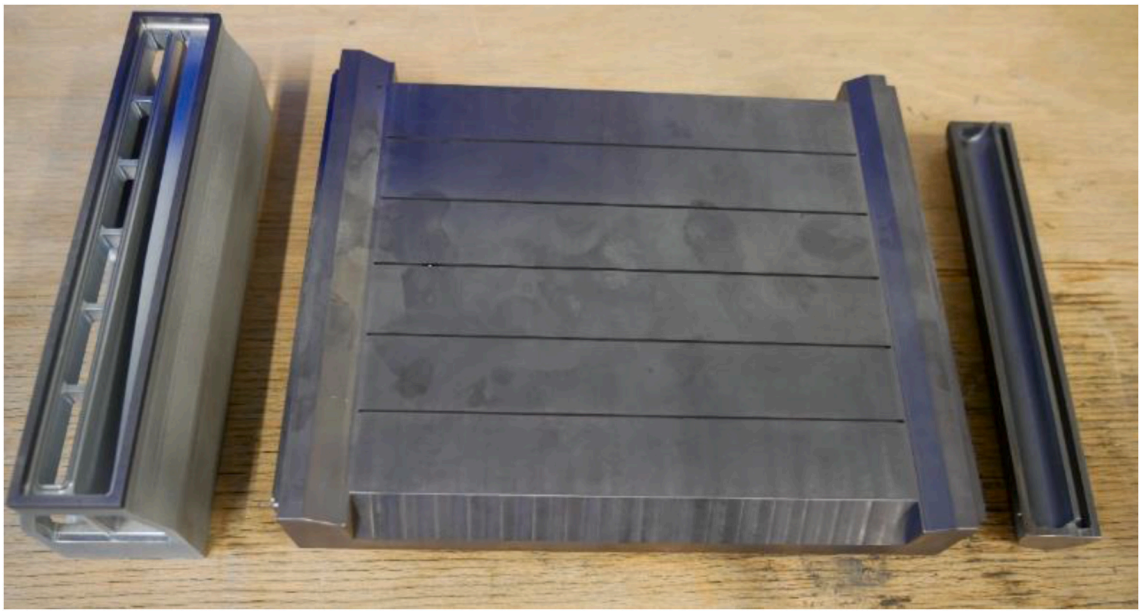

Fig. 23. Machined parts prepared for electron beam welding. Left: Aluminum-Tantal bi-metal adapter, middle: main tantalum body, right: flow deflection

of 4 m/min delivered a reliable weld root in the present configuration, see Fig. 18, left. The determined joining parameters are to be applied to the first full-scale demonstrator.

The achieved welding depth is approximately 0.9 mm. From the structural mechanic point of view this welding depth at the bimetal joint seems to be acceptable because the yield strength of the used, adjacent aluminum alloy ($R_{p\,min}$(AlMg3) = 80 MPa [14,15], or 122 MPa from material certificate of used plate) is considerably lower than those of used tantalum (R_p(Ta) = 213.5 MPa). In contrast, a complete reduction of the wall thickness of the bimetal adapter would most likely not be possible, since the wall thickness of the aluminum would also be reduced and thus the load-bearing capacity would not withstand the coolant pressure. However, if it should be necessary to fully penetrate the wall, e.g. due to a requirement of the applicable directive, the tantalum layer must be enlarged, welding parameters adjusted, and the welding tests repeated.

To verify the influence of the selected welding parameters on the bimetal joint, a cross-section analysis was performed after electron beam welding. No change in the diffusion zone was observed at the Al/Ta-bimetal transition zone, see Fig. 19, middle. Tantalum is annealed by the heat of the welding process and loses the graininess, which is visible in its initial state, see Fig. 19, right. The same holds true for AlMg3 in the immediate vicinity of the bimetal bond, see Fig. 19, left.

After the joining tests were completed, several non-destructive tests (NDT) were carried out to check the quality of the welds. The surface check and square view examinations were without any defects. The leak rate achieved in the helium leak test, before and after pressure test, is $q_L \leq 1 \bullet 10^{-9}$ mbar l/s and fulfill the requirements. The pressure test, with a test pressure of $p = 1.43 \cdot p_o \approx 10$ bar (operation pressure = 6.5 bar), was also without any findings.

With that the initial joining tests are completed and the first full-scale manufacturing test of the HBS Target can be carried out, which will be explained in more detail in the following chapter.

4. Full-scale manufacturing test

Based on the particle-transport and thermo-mechanical simulations, welding qualification and in consultation with mechanical manufacturing, a final design of the tantalum Target structure was generated. Fig. 20 shows the welding drawing of this Target prototype. Fig. 21 shows the manufacturing sequence to produce the first

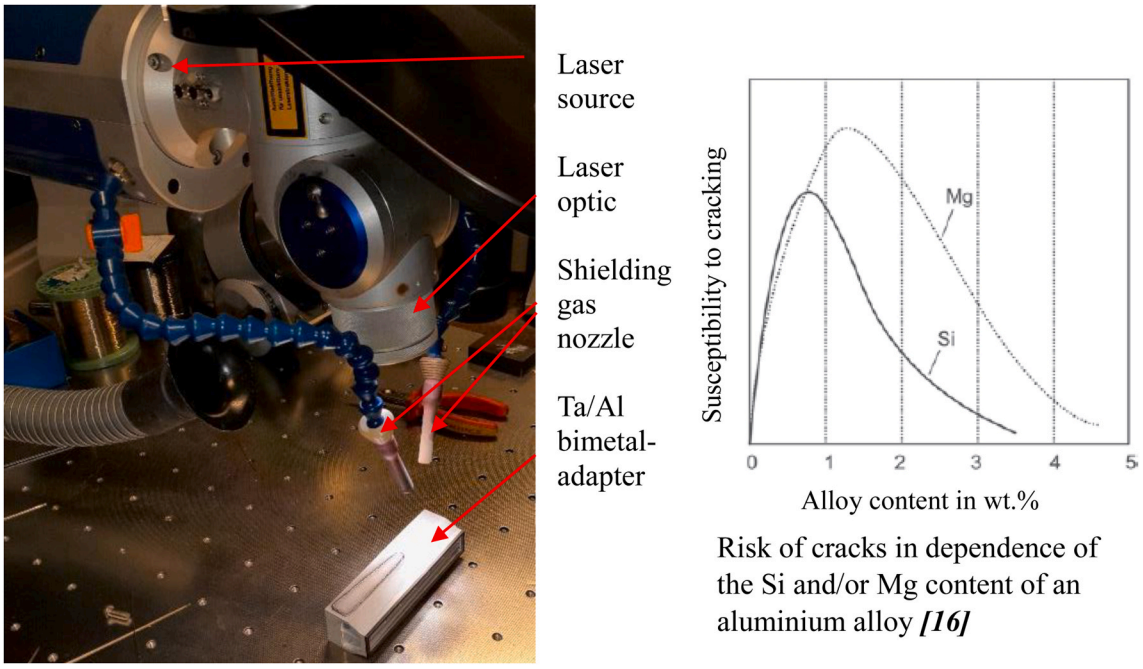

Fig. 24. Ta/Al bimetal adapter at laser beam workstation (left); importance of Si/Mg content (right) [16]

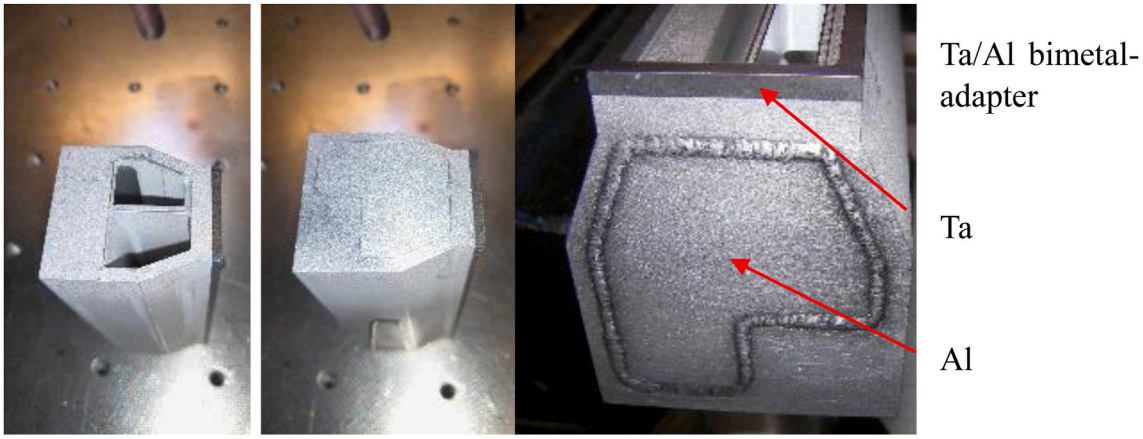

Fig. 25. Ta/Al bimetal adapter; laser beam welding of coverings

tantalum Target prototype, which is explained in detail below.

In order to enable the welding processes, deviations in mechanical manufacturing must be very narrowly limited – beam welding requires a near zero gap for best results.

4.1. Mechanical manufacturing

In order to produce the microchannel cooling structure by wire Electrical Discharge Machining (EDM), starting holes into which the cutting wire can be inserted must first be machined. The start holes of 0.9 mm diameter of each microchannel sector are produced by sink EDM using multi-channel brass electrodes with 0.8 mm diameter. Under high water pressure, the electrode is moved up and down in a spiral shape, which flushes out the material that has been contactless removed. In the next step, the wire coated with Gamma-Brass with a diameter of 0.1 mm, is inserted into the start holes. This wire from the company MICRO-CUT®SF has a high tensile strength of 600 MPa and was necessary because the standard wires broke during processing. Then the micro-channels, with a width of 0.35 mm, are machined out sector by sector, as can be seen in Fig. 22. Finally, the beam stop pocket is also produced by wire EDM machining.

The outer contour of the main tantalum body, the tantalum flow deflection and the Al/Ta-bimetal adapter were finally manufactured by milling, as can be seen in Fig. 23.

4.2. Welding

After processing, all parts were cleaned and degreased by surface technology methods. The covers on the Ta/Al bimetal adapter were welded by manual laser beam welding. This way, the important tack welding and sealing welding with additional filler wire in a diameter of 0.4 mm can be performed on the same device and immediately after each other, see Fig. 24 and Fig. 25. The parts made of AlMg3 are welded with manually added filler wire made of AlSi12. Due to the risk of

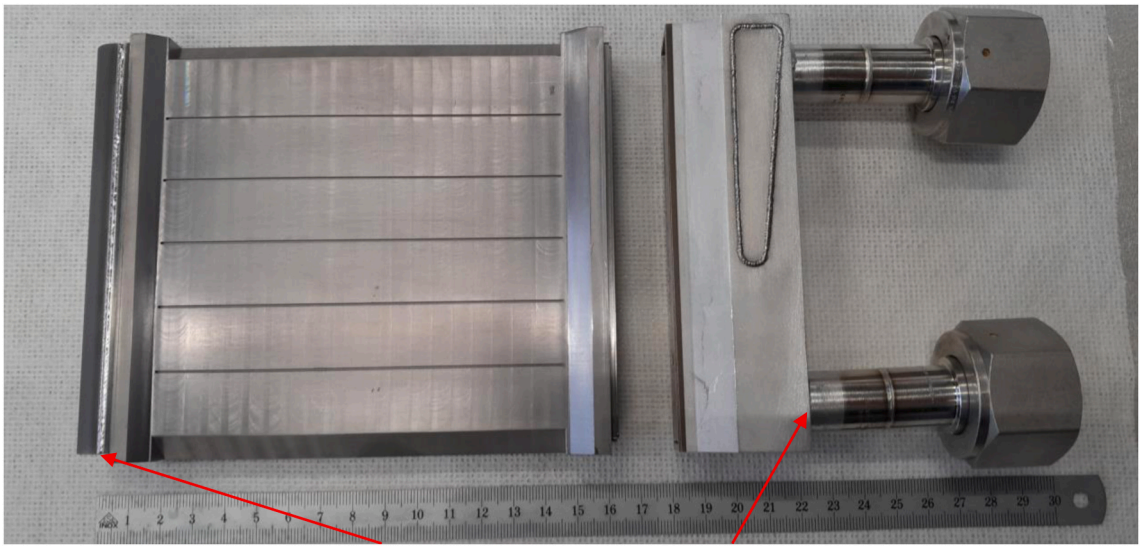

Fig. 26. Target pre welding; flow deflector to main Ta body; water cooling tubes and bimetal adapter

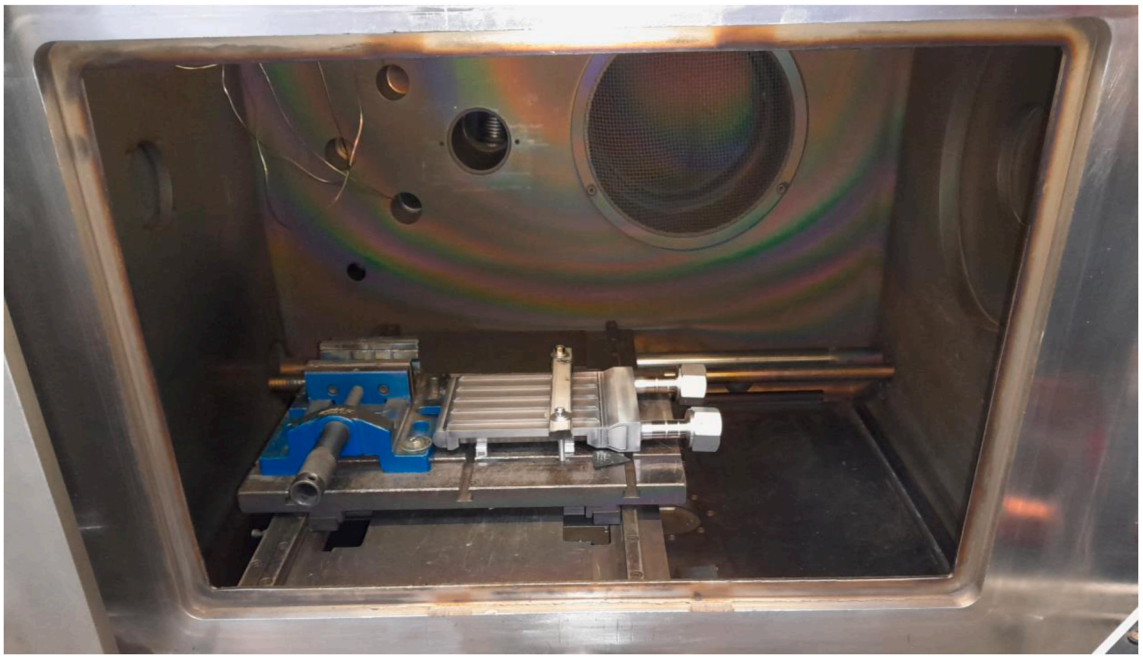

Fig. 27. Target final EBW; fixed on x/y table in EB machine EBW300

microcracks, the additional filler wire is also essential for the AlMg3 alloy. Although it is generally considered to be easily weldable, there is an excessive magnesium vaporization in the melting zone, resulting in a significant increase in crack sensitivity. Therefore, in the production of vacuum components, the use of high-alloy welding filler materials such as AlMg5 or AlSi12 has proven to be very effective. All aluminum welds achieved the leakage rate of the joining zone of $q_L \leq 10^{-9}$ mbar l/s.

Finally, all pre-welded parts had to be assembled to the final body as can be seen in Fig. 26.

Pre-fixing was done by laser tack-welding, and the Target was in the last steps finalized in the electron-beam welding machine. All roots could be done by using the internal x/y-device, see Fig. 27 and Fig. 28.

Fig. 29 shows the final prototype of the HBS tantalum Target.

After the first prototype was completed, non-destructive tests (NDT) were carried out to check the quality of the Target. First, a helium leak test was performed, were a total leakage rate of $q_L \leq 1 \bullet 10^{-9}$ mbar l/s was achieved. Next, a dye penetration test to check if any surface cracks are present were done, with the result that no defects were observed. Finally, a pressure test, with a test pressure of $p = 1.43 \cdot po \approx 10$ bar (operation pressure = 6.5 bar) was done, also without any findings. This proves that the first prototype meets the requirements and therefore the manufacturing feasibility study was successful.

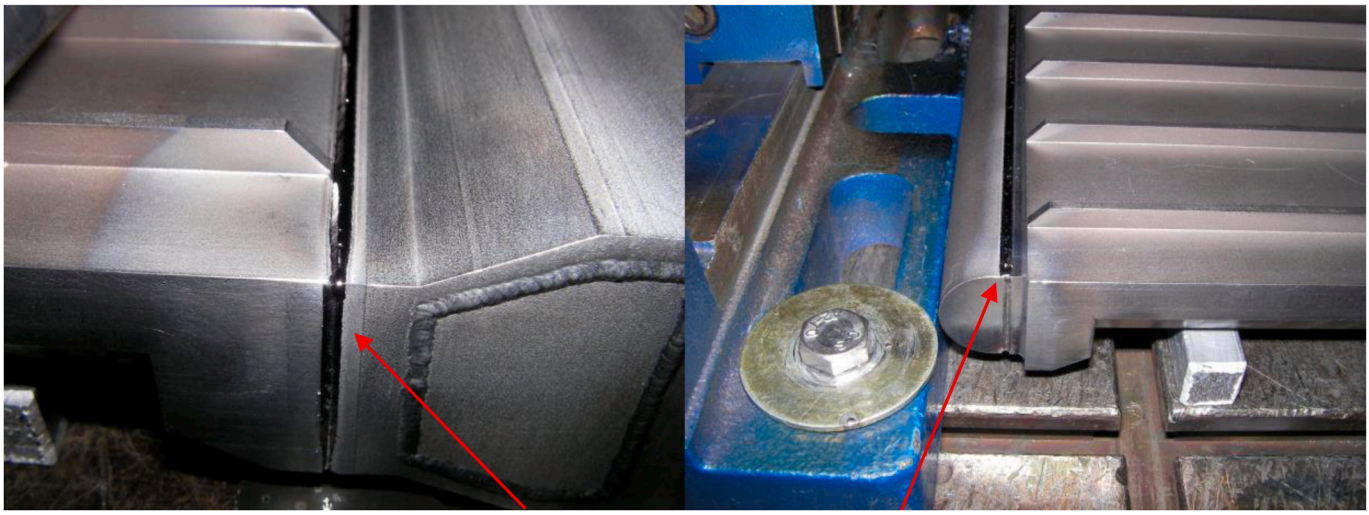

Fig. 28. Details of final EBW-roots; Al/Ta adapter to Ta body; flow deflector to Ta body

Fig. 29. Final manufactured HBS tantalum Target prototype (backside)

5. Summary & outlook

The present feasibility study showed that the complex tantalum Target for the High Brilliance Neutron Source HBS under full load is feasible in principle, both thermo-mechanically and in terms of manufacturing. Even though the final mechanical design, according to the applicable directive, is still pending and may require minor changes in the design, welding and manufacturing processes, the first Target could be successfully produced. As can be seen from the thermo-mechanical simulations, the Target cannot be realized with conventional cooling. Only through the innovative cooling concept based on a microchannel structure in combination with special manufacturing processes, was it possible to meet all requirements in terms of neutronic performance [2] as well as coolability and manufacturability. To ensure that the theoretical assumptions on which the cooling design is based are sufficiently correct, further experimental investigations are planned where the microchannel cooling structure will be tested under realistic conditions. Therefore, in the next step, the produced Target will be subjected to a load test under which a high-energy electron beam will load the Target surface with 100 kW in order to gain practical experience with the microchannel cooling concept. Additionally, the bimetal adapter was used to reduce the amount of tantalum and thus significantly reduce the amount of long-radiating material to be stored. However, no data on irradiated samples are available for this type of bimetal joints, which is why its suitability in a radiation environment still needs to be verified.

The aim of the HBS is to build an innovative and compact, accelerator-driven neutron source with a high brilliance neutron beam that will open up new possibilities for the material- and life-sciences and ensure the regional supply of important medical radioisotopes that are produced in the HBS facility. This publication was created as part of the HBS preliminary study, which, among other things, examined critical components in advance with regard to their feasibility. The next step (still subject to financing) is the design, manufacture, and commission of the first stage of the HBS (HBS-I) with a reduced proton beam of 20 MeV. The design phase of this project is expected to begin immediately after funding is released, but not before 2026/27. The construction phase is scheduled to begin one year after funding is released and will last approximately three years. The start of the operation phase with user operation for scientific and industrial purposes is foreseen around one year after completion of the construction. An upgrade of the HBS-I to the large-scale user facility HBS-II is planned by upgrading the accelerator from 20 MeV to 70 MeV and adding two additional TMR units, each with its own set of neutron instruments.

CRediT authorship contribution statement

Y. Bessler: Writing – original draft. **W. Behr:** Writing – original draft. **S. Rath:** Writing – original draft. **J. Wolters:** Writing – original draft. **J. Baggemann:** Writing – review & editing. **Q. Ding:** Writing – review & editing. **P. Zakalek:** Writing – review & editing. **G. Natour:** Writing – review & editing.

Declaration of competing interest

The authors declare that they have no known competing financial interests or personal relationships that could have appeared to influence the work reported in this paper.

Data availability

Data will be made available on request.

References

[1] J. Baggemann, E. Mauerhofer, et al., Technical design report HBS volume 2 – target stations and moderators. Schriften Des Forschungszentrums Jülich, Band/Volume 9-02, 2023, 978-3-95806-710-3.
[2] Q. Ding, Theoretical Optimization and Experimental Validation of a Microchannel Target for a high-current accelerator-driven Neutron Source, RWTH Aachen University, Aachen, Dissertation, 2023, https://doi.org/10.34734/FZJ-2023-03037.
[3] J. Baggemann, T. Gutberl, et al., High power target for the high brilliance neutron source, Nuclear Inst. and Methods in Physics Research, A (2024), https://doi.org/10.1016/j.nima.2024.169912.
[4] P. Zakalek, P.-E. Doege, et al., Energy and target material dependence of the neutron yield induced by proton and deuteron bombardment, EPJ Web Conf. 231 (2020) 2020, https://doi.org/10.1051/epjconf/202023103006.
[5] T.S. Byun, S.A. Maloy, Dose dependence of mechanical properties in tantalum and tantalum alloys after low temperature irradiation, J. Nucl. Mater. 377 (Issue 1) (2008) 72–79, https://doi.org/10.1016/j.jnucmat.2008.02.034, 30 June 2008.
[6] J. Chen, H. Ullmaier, et al., Mechanical properties of pure tantalum after 800 MeV proton irradiation, J. Nucl. Mater. 298 (3) (2001) 248–254, https://doi.org/10.1016/S0022-3115(01)00654-7. October 2001.
[7] International Association for the Properties of Water and Steam, IAPWS R6-95, Revised Release on the IAPWS Formulation 1995 for the Thermodynamic Properties of Ordinary Water Substance for General and Scientific Use, 2018.
[8] Jahm Software Inc, Material Properties Database, MPDB v9.91, 2025.
[9] H. Ullmaier, Design Properties of Tantalum or Everything You Always Wanted to Know About Tantalum but Were Afraid to Ask, 2003. ESS (European Spallation Source) report ISSN: 1433-559X, 03-131-T.
[10] S. Rath, S. Schneider, Innovative Anwendungsmöglichkeiten Einer Vielfach Unbekannten Technologie - Das Sprengplattieren; Tagungsband: 26. Schweißtechnische Tagung, SLV Halle Gmbh, 2016.
[11] M. Ahlavadi, DetaClad™ (Explosion Cladding)& DetaPipe™ - Clad Solutions for Nitric Acid and Nitrates, 2024.
[12] S. Schiller, U. Heisig, S. Panzer, Electron Beam Technology, Wissenschaftliche Verlagsgesellschaft, 1982. Stuttgart 1977; ISBN: 978-0471060567.
[13] H. Schultz, Elektronenstrahlschweißen, DVS-Verlag, 2017, 978-3-945023-85-3. Düsseldorf 2000.
[14] AFCEN, Rcc-MRx Design And Construction rules FOR Mechanical Components Of Nuclear Installations, 2012 Edition, AFCEN, Lyon, 2012, 2-913638-40-6.
[15] Pressure Equipment Directive (PED) 2014/68/EU (formerly 97/23/EC) of the EU; The Standards for the Design and Fabrication of Pressure Equipment.
[16] F. Ostermann, Anwendungstechnologie Aluminium, Auflage 2, Springer Berlin Heidelberg, New York, 2007, 978-3-540-71196-4.